Iterative Tomographic Image Reconstruction Using Fourier-Based Forward and Back-Projectors

Samuel Matej, *Senior Member, IEEE*, Jeffrey A. Fessler, *Senior Member, IEEE*, and Ivan G. Kazantsev, *Member, IEEE*

***Abstract*— Iterative image reconstruction algorithms play an increasingly important role in modern tomographic systems, especially in emission tomography. With the fast increase of the sizes of the tomographic data, reduction of the computation demands of the reconstruction algorithms is of great importance. Fourier-based forward and back-projection methods have the potential to considerably reduce the computation time in iterative reconstruction. Additional substantial speed-up of those approaches can be obtained utilizing powerful and cheap off-the-shelf FFT processing hardware. The Fourier reconstruction approaches are based on the relationship between the Fourier transform of the image and Fourier transformation of the parallel-ray projections. The critical two steps are the estimations of the samples of the projection transform, on the central section through the origin of Fourier space, from the samples of the transform of the image, and vice versa for back-projection. Interpolation errors are a limitation of Fourier-based reconstruction methods. We have applied min-max optimized Kaiser-Bessel interpolation within the non-uniform Fast Fourier transform (NUFFT) framework. This approach is particularly well suited to the geometries of PET scanners. Numerical and computer simulation results show that the min-max NUFFT approach provides substantially lower approximation errors in tomographic forward and back-projection than conventional interpolation methods, and that it is a viable candidate for fast iterative image reconstruction.**

***Index Terms*— Iterative tomographic reconstruction, forward and back-projectors, non-uniform FFT, gridding, min-max interpolation.**

I. Introduction

IT has been known for a long time that direct Fourier methods (DFM), that build up the Fourier transform of the object using the Fourier transforms of the projections [1]–[6], have the potential for accurate and high speed reconstruction. The Fourier-slice theorem was later proposed to be used as a tool for the reprojection (e.g., [7], [8]). The crucial step in uencing the reconstruction quality and speed is the interpolation between polar and Cartesian rasters in frequency space. Gridding interpolation [9], [10], with proper interpolating [11] and data weighting functions, as investigated in the MRI literature [12]–[14], brought improvement in the direct Fourier reconstruction. Recently, the Fourier-based reprojection has been applied for (noniterative) fully 3D PET reconstruction [15] and for calculation of attenuation correction factors in PET [16]. In these works, Kaiser-Bessel (KB) windows were used for interpolation, which are known to be reasonably accurate [9] but without explicitly evaluating the accuracy. The concept of the non-uniform Fast Fourier transform (NUFFT) [17] used in this paper is related to gridding methods for interpolation in frequency space. The KB interpolation kernels used in this work have been optimized using a min-max approach [18], thus providing substantial improvement of the interpolation accuracy.

In the previous works on gridding, the focus was on using the interpolation to nd a non-iterative approximate solution to an inverse problem. In contrast, we use Fourier-based forward-projection as a tool for calculating the forward problem, and allow iterative reconstruction methods to solve the inverse problem. Iterative algorithms need also the ability to compute matrix-vector multiplication by the transpose of that matrix, even though the matrix itself is not stored explicitly. It is straightforward to reverse (not invert) the steps executed during the forward-projection computation (see Fig. 1) to develop an algorithm to perform multiplication by the transpose, corresponding to the adjoint of the forward operator, which is a form of back-projection.

II. Non-Uniform Fast Fourier Transform

In the NUFFT method the input signal is given on the uniform grid and the output signal is calculated on the non-uniform grid of frequency locations. Applying the NUFFT for calculation of the forward-projection within iterative tomographic reconstruction, the input signal represents an image de ned on the regular grid and the output signal represents the frequency spectrum of the projections located on the polar raster (in the 2D case), as given by the projection slice theorem [2]. The projections are then obtained by inverse Fourier transformation of the spectrum values located on the polar lines. Direct evaluation of the samples on the spectrum grid using nonuniform discrete Fourier transform (NDFT) would require $O(N^4)$ operations for the 2D case. Nonuniform FFT allows to substantially speed-up this process by requiring only $O(N^2 \log N)$ operations, compared to $O(N^3)$ needed by the spatial forward-projection algorithms. Basic steps of the NUFFT Forward-projection are (see Fig. 1):

Manuscript received November 15, 2002. This work was supported by NIH grants CA-92060, CA-60711 and by The Whitaker Foundation.

S. Matej and I. G. Kazantsev are with the Department of Radiology, University of Pennsylvania, Philadelphia, PA 19104-6021 USA (telephone: 215-662-6780, e-mail: {matej,kazantsev}@mipg.upenn.edu)

J. A. Fessler is with the Electrical Engineering and Computer Science Department, University of Michigan, Ann Arbor, MI 48109-2122 (telephone: 734-763-1434, e-mail: fessler@umich.edu)

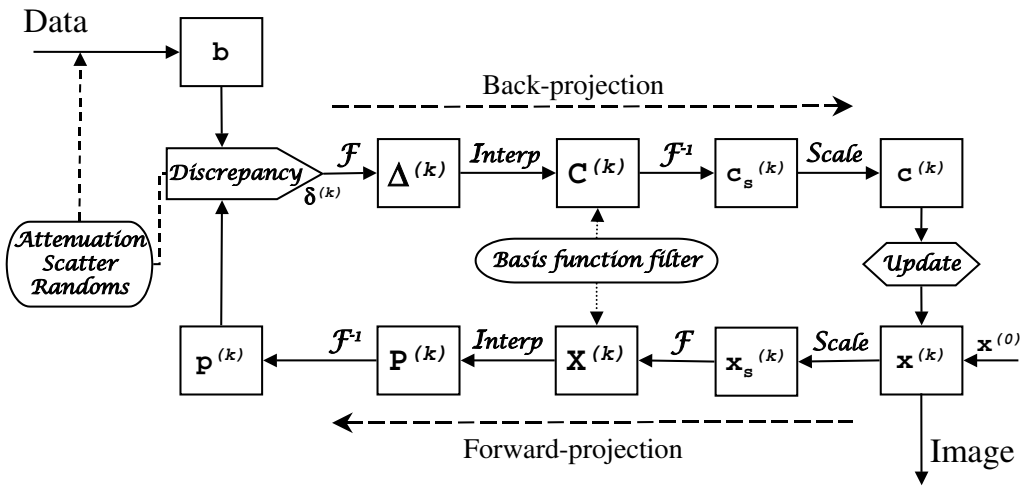

Fig. 1. Flowchart of iterative reconstruction using Fourier-based forward and back-projection. $Discrepancy$ and $Update$ operators are de ned by a particular iterative technique. For the 2D case, the Fourier transformations are 1D (I)FT of projections on data side and 2D (I)FT on image side. $Interpolation$ operations are performed between data (polar) and image (rectangular) spectrum grids. $Scale$, also known as the "correction function" in the gridding, is scaling operation, where the scaling factors are designed to compensate for imperfections (departure from the ideal Sinc interpolation) in the interpolation step. $Basicfunctionfilter$ is spectral operation allowing ef cient modeling of image basis function and detector resolution kernel.

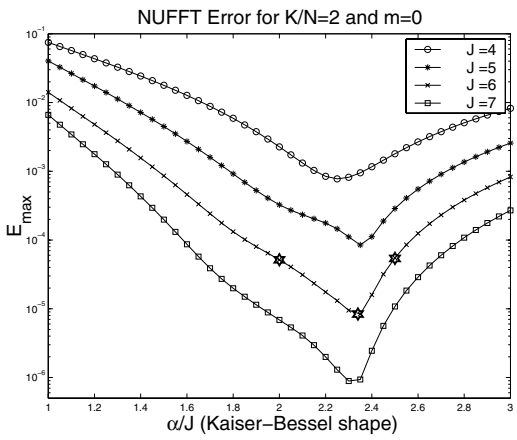

Fig. 2. Maximum error ε_{max} of Kaiser-Bessel interpolator as a function of the shape parameter α, for several interpolation kernel sizes J, Bessel order $m = 0$ and using 100% zero-padding of the spatial domain ($K/N = 2$) (NUFFT interpolator has been found to perform best for the KB orders close to $m = 0$ - see Fig. 3). Note that the optimum ratio α/J is about 2.34 for varying kernel sizes.

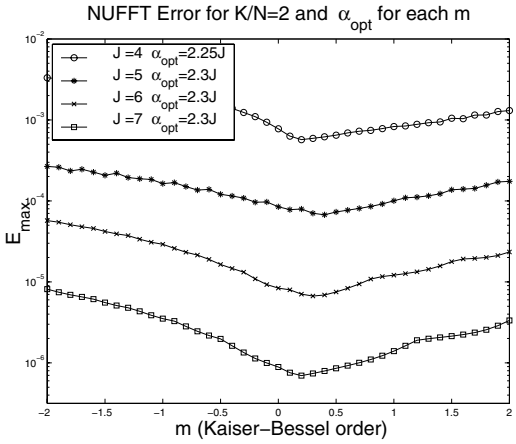

Fig. 3. Maximum error ε_{max} of Kaiser-Bessel interpolator as a function of the order m, for several sizes J, 100% zero-padding ($K/N = 2$) and using optimum ratio α/J for each particular value of m. The optimum order parameter m is slightly above 0 for all kernel sizes; α_{opt} in the legend represent global optimum of the α parameter for the given kernel size.

- image of size N is rst pre-compensated (*scaled*) for imperfections for the subsequent frequency domain interpolation;
- calculation of the K-times oversampled FFT (image is zeropadded before the FFT - for the ef cient implemention of the oversampled FFT see [18], Section III-D);
- interpolation onto the desired nonuniform frequency locations using small local neighborhoods in the frequency domain;
- inverse FFTs on polar lines to obtain projections.

The discrete backprojection represents the same set of operations executed in the reverse order. The crucial step for the quality of the NUFFT is interpolation. We have utilized Kaiser-Bessel (KB) interpolation kernel [19] which was optimized to be optimal in the min-max sense of minimizing the worst-case approximation error over all signals of unit norm using the methodology described in [18].

III. Numerical Error Analysis

We have calculated maximum error ε_{max} for the range of oversampling factors ($K/N = 1, 1.5, 2, 3$), interpolation kernel sizes ($J = 4, 5, 6, 7$), orders of KB window ($m = -2, ..., 2$) and KB shape (width) parameter (α, where $\alpha/J = 1, ..., 3$). The interpolation error is rapidly decreasing with the amount of oversampling. We show only results (Figs. 2, 3, 4) for the case $K/N = 2$ (a reasonable compromise between the speed and quality). Behavior for other oversampling cases is similar. The optimum order of the KB interpolator is close to zero for all K/N, contrary to our previous experiences with the KB window used as spatial image basis function [20]. At $m = 0$, optimal values of α/J ratio are approximately constant over range of KB kernel sizes (about 1.5 for $K/N = 1$, 2.05 for

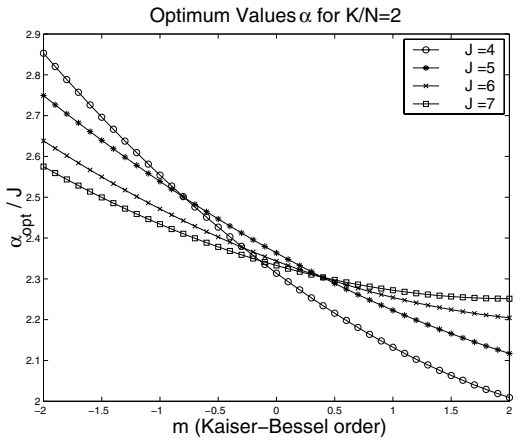

Fig. 4. Values of the optimum ratio (α_{opt}/J) as a function of the KB order m, for 100% zero-padding ($K/N = 2$). The values of optimum ratio for individual kernel sizes cluster around similar value for order $m = 0$ and diverge for other orders. Similar behavior have been observed for other values of K/N, but with different value of the optimum ratio at $m = 0$.

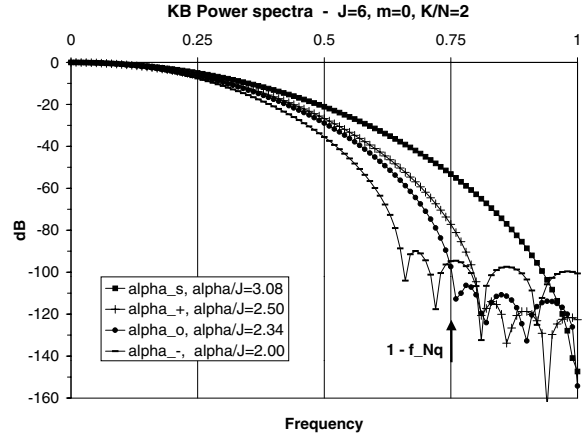

Fig. 5. Power spectra of Kaiser-Bessel interpolation kernels of size $J = 6$ using optimum (*alpha_o*) and suboptimum parameters for $m = 0$ and $K/N = 2$. *alpha_-* and *alpha_+* represent two subotimum KB kernels (α parameter located on both sides from the optimum - star symbols in Fig. 2) providing comparable maximum errors, which are about 6.5-times higher than in the optimum case. For comparison, we show also *alpha_s* representing typical KB window having desirable properties for the spatial image representation [20], but poor performance as the interpolation kernel.

$K/N = 1.5$, 2.34 for $K/N = 2$ and 2.6 for $K/N = 3$).

Figs. 5 and 6 show power spectra and pro les, respectively, of optimal and suboptimal interpolation kernels. Note that the reciprocal (spectral) domain for the NUFFT interpolators is the spatial image domain. Consequently, the frequency 1.0 represents repetition image period given by the spectrum sampling and *1-f_Nq* represents periodic repeat of the (left) image boundary for the case of 100% oversampling ($K/N = 2$), beyond which the interpolation kernel spectrum should be effectively zero. Optimum interpolation kernel is a compromise between the requirements that the main lobe of its transform (spectrum) decays to negligible values at, or before, the image periodic repeat *1-f_Nq* (limiting α from the top) and that its side

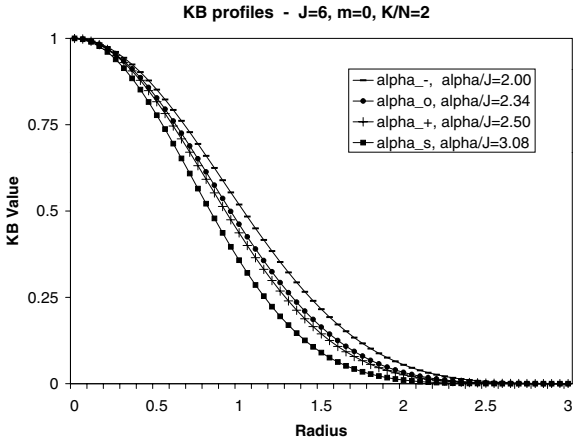

Fig. 6. Pro les of four Kaiser-Bessel interpolation kernels of size $J = 6$ using optimum (*alpha_o*) and suboptimum parameters for $m = 0$ and $K/N = 2$ (see Fig. 5). It is interesting that although all of them have similar shape, they provide quite dramatic difference in the NUFFT performance.

lobes are effectively zero beyond that point (requiring large α). Any deviation from this compromise leads to a dramatic increase of the interpolation errors (see star symbols in Fig. 2), inspite of a very similar kernel shapes (Fig. 6).

IV. Computer Simulation Results

A. Forward-Projector

Additionally to numerical evaluation of NUFFT-based forward projector for the worst case error, we have evaluated the accuracy of the NUFFT-based forward projector using Zubal digital phantom. The image size have been limited to 100x100 pixels (from 128x128) so that the phantom torso fully occupies the whole image region in its wider dimension (to avoid any extra zero-padding, other than that given by K/N). We have simulated a parallel-beam tomographic system, with a sinogram size of 100 radial bins by 192 angles over 180°, including a rectangular detector response $h(r) = \text{rect}(r)$ with width equal to the pixel size, partially representing the nite detector width in a PET system (rather than using overly idealized line integrals). We have computed forward projections of this object in three ways: using Fourier-based reprojection with exact (to within double precision in Matlab) evaluation of the 2D FT, using Fourier-based reprojection with the 2D NUFFT approximation to using min-max optimized Kaiser-Bessel interpolation and using a bilinear interpolation. Based on the difference between the exact FT and NUFFT method we have evaluated Maximum Error, Root Mean Square Error and Mean Error. We show only maximum error de ned as the maximum absolute difference between exact FT and NUFFT method in percent of the maximum value of the exact FT method. Other errors have been found to exhibit similar behavior. The errors have been evaluated for the same set of the NUFFT parameters as in the numerical analysis. Error curves as function of the α (Fig. 7) show very similar behavior to the numerical case, with nearly exactly same optima. The optima over m (Fig. 8)

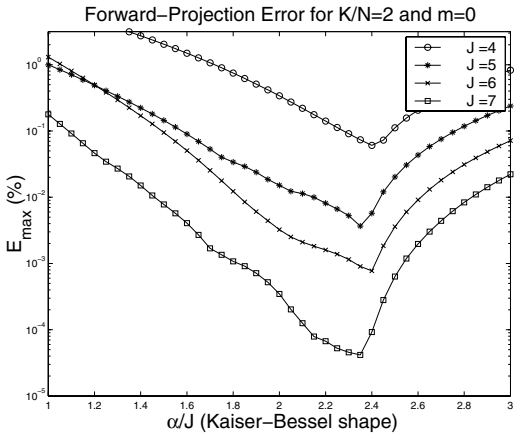

Fig. 7. Maximum interpolation error (% of projection maximum) of forward-projection of modi ed Zubal phantom using NUFFT with Kaiser-Bessel interpolator of several sizes J as a function of the parameter α. Same set of parameters used as for the Fig. 2

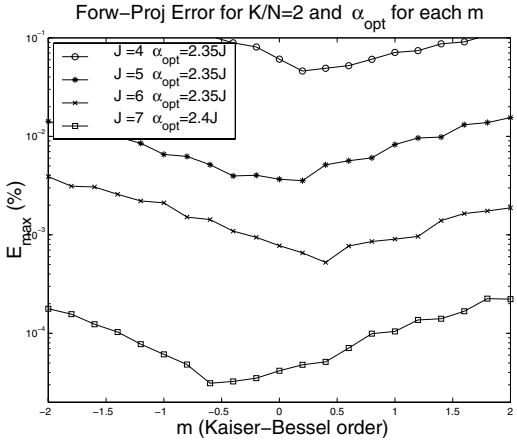

Fig. 8. Maximum interpolation error (% of projection maximum) of forward-projection of modi ed Zubal phantom using NUFFT with Kaiser-Bessel interpolator of several sizes J as a function of the KB order m. For each individual m an optimum α was used. α_{opt} in the legend represent global optimum of the α parameter for the given kernel size.

are less consistent compared to the theoretical case (Fig. 3) but the locations of the minimum of the worst case error E_{max} are still clustered around the $m = 0$. The calculated sinograms for the optimum values are visually indistinguishable (from the exact FT approach) with errors smaller than 0.06% for the K/N even for the smallest kernel size ($J = 4$). By comparison, conventional bi-linear interpolation for the polar to cartesian conversion gives about two orders of magnitude higher maximum error for this choice of J.

B. Back-Projector

The adjoint operator (back-projector) of the NUFFT-based forward projector using the Kaiser-Bessel interpolator have been compared to the adjoint of the exact Fourier-based re-projector when applied to a ramp- ltered ideal sinograms of the modi ed Zubal phantom. The maximum error have been

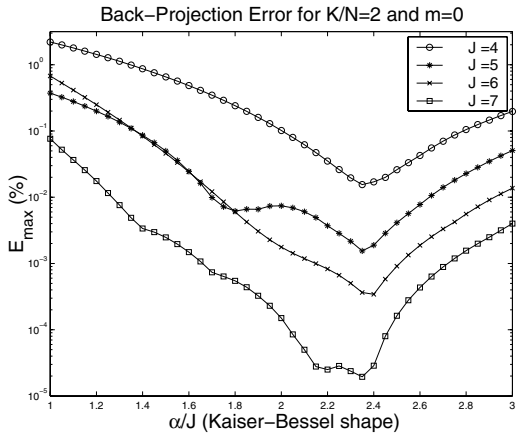

Fig. 9. Maximum interpolation error (% of phantom maximum) of discrete back-projection using NUFFT with Kaiser-Bessel interpolator of several sizes J as a function of the parameter α. Same set of parameters used as for the Figs. 2, 7.

calculated within the phantom torso region as the percent error of the maximum value in the Zubal phantom. Again, the error curves (Fig. 9) are consistent with the previous cases and the NUFFT approach agrees with the exact approach within 0.016%, even for the smallest kernel size ($J = 4$). Similar behavior to forward-projection case have been observed also for the error as the function of m.

C. Forward and Back-Projector within Iterative Reconstruction

Since iterative algorithms require repeated forward and back-projections, it is conceivable that even small errors in the reprojector could accumulate. To study practical performance of the NUFFT forward and back-projector within the iterative reconstruction following experiments have been performed. We have simulated noisy PET sinogram measurements (including attenuation, randoms and scatter) from the 128x128 Zubal phantom shown in Fig. 11. We have simulated a parallel-beam

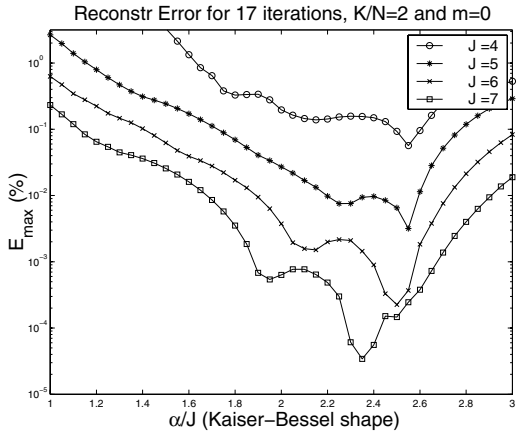

Fig. 10. Maximum interpolation error (% of phantom maximum) of 17 iterations of QPWLS reconstruction using NUFFT forward and back-projectors with Kaiser-Bessel interpolator of several sizes J as a function of the parameter α. Same set of interpolation parameters used as for the Figs. 2, 7, 9.

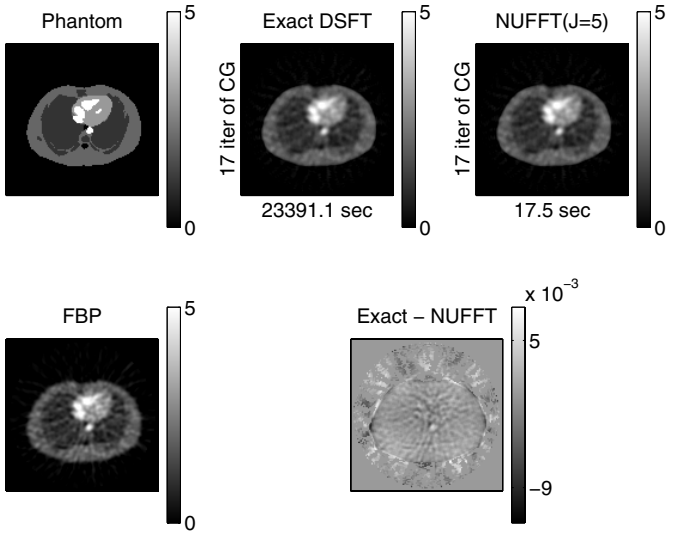

Fig. 11. FBP and QPWLS-CG reconstructions (17 iterations) of thorax phantom using exact and NUFFT Fourier-based forward and back-projectors. Parameters used for the NUFFT were $K/N = 2$, $m = 0$, $J = 5$, and $\alpha/J = 2.34$. The maximum error within the torso region was 0.009%. Note that the α used in this example has been chosen based on the theoretical min-max optimization and not based on the experimental optimization for the particular data set.

tomographic system with a sinogram size of 160 radial bins by 192 angles over 180° with a rectangular detector response $h(r) = \text{rect}(r)$ of equivalent width to the pixel size. We have run 17 iterations of the conjugate gradient algorithm for a data-weighted least-squares cost function [21] with a standard quadratic rst-order roughness penalty. The same set of the NUFFT parameters have been used as in the previous cases and the results have been compared to the reconstruction using exact Fourier-based forward and back-projector. The maximum error have been calculated within the phantom torso region as the percent error of the maximum value in the phantom. The error curves show again similar behavior, with the optimum slightly shifted towards higher alpha values. This is probably caused by the fact that the phantom does not cover the whole image region (causing an additional zero-padding). The maximum error is below 0.06% even for the smallest kernel size ($J = 4$).

Fig. 11 illustrates that the reconstructed images using exact FT and NUFFT interpolators are visually indistinguishable. The difference between the FBP image and the QPWLS-CG image is not so dramatic in this 2D example. We expect that the difference would be more signi cant for 3D acquisitions.

V. Conclusions

Our results show a very good agreement of the theoretical min-max error analysis of the NUFFT forward and back-projectors with their practical performance. We nd that the min-max approach is an excellent framework for the optimization of the NUFFT interpolation parameters. Our results further demonstrate that the NUFFT based forward and back-projectors with the min-max optimized Kaiser-Bessel interpolation are fast and extremely accurate and are therefore viable tools for iterative tomographic reconstruction.

Acknowledgments

The authors gratefully acknowledge Robert M. Lewitt for fruitful discussions and comments on this work.

References

[1] R. M. Lewitt, "Reconstruction algorithms: Transform methods," *Proc. IEEE*, vol. 71, no. 3, pp. 390–408, 1983.

[2] A. C. Kak and M. Slaney, *Principles of Computerized Tomographic Imaging*, IEEE Press, New York, 1987.

[3] N. Niki, R. T. Mizutani, Y. Takahashi, and T. Inouye, "A high-speed computerized tomography image reconstruction using direct two-dimensional Fourier transform method," *Syst. Comput. Controls*, vol. 14, no. 3, pp. 56–65, 1983.

[4] S. Matej and I. Bajla, "A high-speed reconstruction from projections using direct Fourier method with optimized parameters - an experimental analysis," *IEEE Trans. Med. Imaging*, vol. 9, no. 4, pp. 421–429, 1990.

[5] M. Magnusson, P. E. Danielsson, and P. Edholm, "Artefacts and remedies in direct Fourier reconstruction," in *Proceedings of the 1992 IEEE Nuclear Science Symposium and Medical Imaging Conference, vol.2*. Orlando, Florida, 1992, pp. 1138–1140.

[6] H. Schomberg and J. Timmer, "The gridding method for image reconstruction by Fourier transformation," *IEEE Trans. Med. Imaging*, vol. 14, no. 3, pp. 596–607, 1995.

[7] C. W. Stearns, D. A. Chesler, and G. L. Brownell, "Three dimensional image reconstruction in the Fourier domain," *IEEE Trans. Nucl. Sci.*, vol. 34, no. 1, pp. 374–378, 1990.

[8] S. Dunne, S. Napel, and B. Rutt, "Fast reprojection of volume data," in *Proceedings of the First Conference on Visualization in Biomedical Computing*. Atlanta, GA, 1990, pp. 11–18.

[9] J. D. O'Sullivan, "A fast sinc function gridding algorithm for Fourier inversion in computer tomography," *IEEE Trans. Med. Imaging*, vol. 4, no. 4, pp. 200–207, 1985.

[10] H. Sedarat and D. G. Nishimura, "On the optimality of the gridding reconstruction algorithm," *IEEE Trans. Med. Imaging*, vol. 19, no. 4, pp. 306–317, 2000.

[11] J. I. Jackson, C. H. Meyer, D. G. Nishimura, and A. Macovski, "Selection of a convolution function for Fourier inversion using gridding," *IEEE Trans. Med. Imaging*, vol. 10, no. 3, pp. 473–478, 1991.

[12] C. H. Meyer, B. S. Hu, D. G. Nishimura, and A. Macovski, "Fast spiral coronary artery imaging," *Magn. Reson. Med.*, vol. 28, pp. 202–213, 1992.

[13] D. C. Noll, "Multishot rosette trajectories for spectrally selective MR imaging," *IEEE Trans. Med. Imaging*, vol. 16, no. 4, pp. 372–377, 1997.

[14] J. G. Pipe and P. Menon, "Sampling density compensation in MRI: Rationale and an iterative numerical solution," *Magn. Reson. Med.*, vol. 41, no. 1, pp. 179–186, 1999.

[15] S. Matej and R. M. Lewitt, "3D-FRP: Direct Fourier reconstruction with Fourier reprojection for fully 3D PET," *IEEE Trans. Nucl. Sci.*, vol. 48, no. 4, pp. 1378–1385, 2001.

[16] S. Matej, M. E. Daube-Witherspoon, and J. S. Karp, "Performance of 3D RAMLA with smooth basis functions on fully 3D PET data," in *Proceedings of The Sixth International Meeting on Fully Three-Dimensional Image Reconstruction in Radiology and Nuclear Medicine*, R. H. Huesman, Ed. Paci c Grove, CA, 2001, pp. 193–196.

[17] J. A. Fessler and B. P. Sutton, "A min-max approach to the multidimensional nonuniform FFT: Application to tomographic image reconstruction," in *Proc. Intl. Conf. on Image Processing*, 2001, vol. 1, pp. 706–709.

[18] J. A. Fessler and B. P. Sutton, "Nonuniform fast Fourier transforms using min-max interpolation," *IEEE Trans. Signal Processing*, vol. 51, no. 2, 2003, To appear.

[19] R. M. Lewitt, "Multidimensional digital image representations using generalized Kaiser-Bessel window functions," *J. Opt. Soc. Am. A*, vol. 7, no. 10, pp. 1834–1846, 1990.

[20] S. Matej and R. M. Lewitt, "Practical considerations for 3D image reconstruction using spherically-symmetric volume elements," *IEEE Trans. Med. Imaging*, vol. 15, no. 1, pp. 68–78, 1996.

[21] J. A. Fessler, "Penalized weighted least-squares image reconstruction for positron emission tomography," *IEEE Trans. Med. Imaging*, vol. 13, no. 2, pp. 290–300, 1994.